RAPID COMMUNICATION

Synthesis of nitrogen-doped single-walled carbon nanotubes and monitoring of doping by Raman spectroscopy*

Wu Mu-Hong(吴慕鸿)[a)b)], Li Xiao(李 晓)[c)], Pan Ding(潘 鼎)[b)], Liu Lei(刘 磊)[b)], Yang Xiao-Xia(杨晓霞)[b)], Xu Zhi(许 智)[b)], Wang Wen-Long(王文龙)[b)†], Sui Yu(隋 郁)[a)‡], and Bai Xue-Dong(白雪冬)[b)§]

[a)] *Department of Physics, Harbin Institute of Technology, Harbin* 150001, *China*

[b)] *Beijing National Laboratory for Condensed Matter Physics, Institute of Physics, Chinese Academy of Sciences, Beijing* 100190, *China*

[c)] *International Center for Quantum Materials, School of Physics, Peking University, Beijing* 100871, *China*

(Received 23 April 2013; revised manuscript received 20 May 2013)

Nitrogen-doped single-walled carbon nanotubes (CN_x-SWNTs) with tunable dopant concentrations were synthesized by chemical vapor deposition (CVD), and their structure and elemental composition were characterized by using transmission electron microscopy (TEM) in combination with electron energy loss spectroscopy (EELS). By comparing the Raman spectra of pristine and doped nanotubes, we observed the doping-induced Raman G band phonon stiffening and 2D band phonon softening, both of which reflect doping-induced renormalization of the electron and phonon energies in the nanotubes and behave as expected in accord with the n-type doping effect. On the basis of first principles calculations of the distribution of delocalized carrier density in both the pristine and doped nanotubes, we show how the n-type doping occurs when nitrogen heteroatoms are substitutionally incorporated into the honeycomb tube-shell carbon lattice.

Keywords: single-walled carbon nanotubes, nitrogen doping, chemical vapor deposition, Raman spectroscopy

PACS: 61.48.De, 81.15.Gh, 63.22.Gh, 78.30.Na **DOI:** 10.1088/1674-1056/22/8/086101

1. Introduction

A key challenge for the practical applications of carbon nanotubes (CNTs) is the control of their electronic properties. A number of research efforts have been made toward this purpose, such as the post-synthesis sorting of metallic and semiconducting nanotubes,[1,2] controlling the chiralities and thereby the electronic structures of nanotubes during growth,[3,4] and modifying the electronic properties of nanotubes by substitutional doping with heteroatoms.[5–12] Boron (B) and nitrogen (N) are the two practical candidates for chemical doping of CNTs, since they are the nearest neighbors to carbon in the periodic table and their atomic sizes are the most similar to that of carbon. Besides B and N, the experimental investigation of phosphorus (P) doping of CNTs has also been reported.[6] In both theoretical and experimental aspects, the nitrogen-doped CNTs have been studied most. Due to the electron-rich nature of nitrogen dopants, the incorporation of nitrogen heteroatoms into the honeycomb carbon lattice generally leads to the formation of n-type-doped nanotubes that hold promise for applications such as nanotube-based electronic devices, sensors, field-emission tips, and energy-storage materials.[7,8,13] At the same time, the controllably doped CNTs, especially in the form of single-walled nanotubes (SWNTs), can also provide a model system to study charge defect-induced perturbations and/or renormalization of the electron and phonon energies in sp^2-based graphitic carbon systems.[14,15]

Although experimental studies of nitrogen-doped CNTs in the form of multi-walled nanotubes (MWNTs) have been extensively reported over the past years,[7,8,13] synthesis of controllably doped CN_x-SWNTs has proved to be much more difficult and challenging.[7–11] Herein, we present the bulk-quantity synthesis of CN_x-SWNTs through a simple and conventional chemical vapor deposition (CVD) growth procedure by employing methane (CH_4) as the carbon source, ammonia (NH_3) as the nitrogen source, and powdery MgO supported Fe–Mo bimetallic nanoparticles (Fe–Mo/MgO) as catalyst. By adjusting the growth parameters, we are able to grow CN_x-SWNTs with varying dopant concentrations. Raman spectroscopy is employed to examine the effects of nitrogen doping in CN_x-SWNTs, in which D band, G band, and the second-order 2D band are characteristic for carbon-related materials. The stiffening of the G band phonon and softening of the 2D

*Project supported by the National Natural Science Foundation of China (Grant Nos. 11004230, 51172273, 11290161, and 11027402), the National Key Basic Research Program of China (Grant Nos. 2012CB933003 and 2013CB932603), and the Innovative Project of the Chinese Academy of Sciences (Grant No. KJCX2-YW-W35).

†Corresponding author. E-mail: wwl@aphy.iphy.ac.cn

‡Corresponding author. E-mail: suiyu@hit.edu.cn

§Corresponding author. E-mail: xdbai@aphy.iphy.ac.cn

© 2013 Chinese Physical Society and IOP Publishing Ltd

band phonon are observed.[6,10,14] This Raman response reflects the evolution of the electron–phonon interactions, and can be ascribed to the n-type doping effect, similar to that observed in the electrostatic doping of CNTs or graphene by an external gate field.[16–19]

2. Experimental section

2.1. Synthesis of pristine and doped SWNTs

We used the support-type powdery Fe–Mo/MgO (with Fe:Mo = 10:1) catalyst to grow C-SWNTs and CN_x-SWNTs. The detailed procedure of catalyst preparation is the same as that reported in our previous publications.[20,21] The CVD growth was carried out by employing CH_4 and NH_3 gas resources as carbon and nitrogen feedstock, respectively, and argon (Ar) as carrier gas. For C-SWNTs growth, the gas flow was fixed to 100 sccm/200 sccm of CH_4/Ar. As for the growth of CN_x-SWNTs with different dopant concentrations, the gas flows were set to be 90/10/200 sccm of CH_4/NH_3/Ar (with CH_4:NH_3 = 9:1, for low nitrogen doping) and 100/20/200 sccm of CH_4/NH_3/Ar (with CH_4:NH_3 = 5:1, for high doping). Growth conditions were typically 30 minutes of deposition at 900 °C.

2.2. Characterization

The structural characterization of both pristine and N-doped SWNTs was performed by using scanning electron microscopy (SEM, Hitachi S-5200) and transmission electron microscopy (TEM, JEM-2010F). The chemical composition analysis of the samples was carried out by using the electron energy loss spectrum (EELS, Gatan Enfina) integrated in TEM. Raman characterization of the samples was conducted by Raman spectroscopy (Horiba Jobin Yvon YJ-T64000) at room temperature and an atmospheric environment.

3. Theoretical methods

Density-functional theory calculations were performed using the Vienna *ab initio* simulation package (VASP) v 5.2,[22,23] with the exchange–correlation functional described by the Perdew–Burke–Ernzerhof version (PBE) of the gradient generalized approximation (GGA).[24] The projector augmented wave (PAW) pseudopotentials[25] were employed and the energy cutoff for the plane-wave basis set was 600 eV. The supercell under periodic boundary condition was chosen to keep nanotubes at a lateral distance of a minimum of 15 Å, so that the vacuum was sufficient to reduce spurious interaction between nanotubes below a total energy of 3 meV for the 40 atoms in the supercell. The theoretical equilibrium C–C bond length was 1.428 Å. The K-space sampling was performed with the method of Monkhorst and Pack[26] using a $1\times1\times56$ grid for (6, 6) SWNT and a $1\times1\times26$ grid for (10, 0) SWNT. All the considered structures were fully optimized until the forces on each atom were less than 0.01 eV/Å.

3.1. Results and discussion

Figure 1 displays representative SEM and TEM images and EELS spectra of the as-grown pristine and doped SWNTs. From the SEM images, the high density of SWNT bundles entangled with the spent powdery Fe–Mo/MgO catalyst can be clearly observed. Further structural analysis by high-resolution TEM reveals that the as-gown nanotubes are primarily of single-walled tubular structures with diameters mainly in the range of 1 nm–2 nm. In the corresponding EELS spectra shown in Figs. 1(c), 1(f), and 1(i), the sharply defined π^* and σ^* fine structure features of the carbon K-edge are characteristic for the formation of a well-graphitized carbon lattice. In other words, both the pristine and doped SWNTs are well graphitized and therefore of high quality.

The nitrogen K-edge features in the EELS spectra of the doped SWNTs (Figs. 1(f) and 1(i)) are much weaker but clearly discernible, indicating that the nanotubes have been successfully doped by nitrogen heteroatoms. As can be calculated from the EELS elemental quantification, the detected nitrogen dopant concentrations are about 1.67 at% for nanotubes grown with CH_4:NH_3 of 9:1 and are about 2.51 at% for nanotubes grown with CH_4:NH_3 of 5:1, respectively. It can be inferred that with an increase of the NH_3 concentration in the gas source during nanotube growth, the nitrogen doping levels of resultant CN_x-SWNTs can be effectively enhanced. Thus far, there have been a number of theoretical publications concerned with modeling the bonding configuration of nitrogen dopants within the nanotube shell lattice, and three main structural modes have been proposed: pyridine-like, pyrrole-like, and graphitic nitrogen. Experimentally, the pyridinic and graphitic nitrogen are more often detected, as revealed in a number of studies of the CN_x-MWNTs. In a recent study of the N-doped SWNTs grown by the arc-discharge method, Glerup *et al.* observed from the EELS spectra that the nitrogen K-edge exhibits two split weak π^* peaks located at 398.6 eV and 402 eV which can be attributed to the pyridinic and graphitic nitrogen, respectively.[27] In our present study, we also have tried to examine the fine structure of nitrogen K-edge. For low doping level samples, it was nearly impossible to resolve any fine feature of the π^* peaks, while from the EELS data of high doping level samples shown in Fig. 1(i), the existence of pyridinic and graphitic nitrogen features can be discerned (for the magnification of CN_x-SWNTs' EELS nitrogen K-edge, see Fig. 2). It seems that the graphitic form of nitrogen dopants is dominant within the as-grown CN_x-SWNTs.

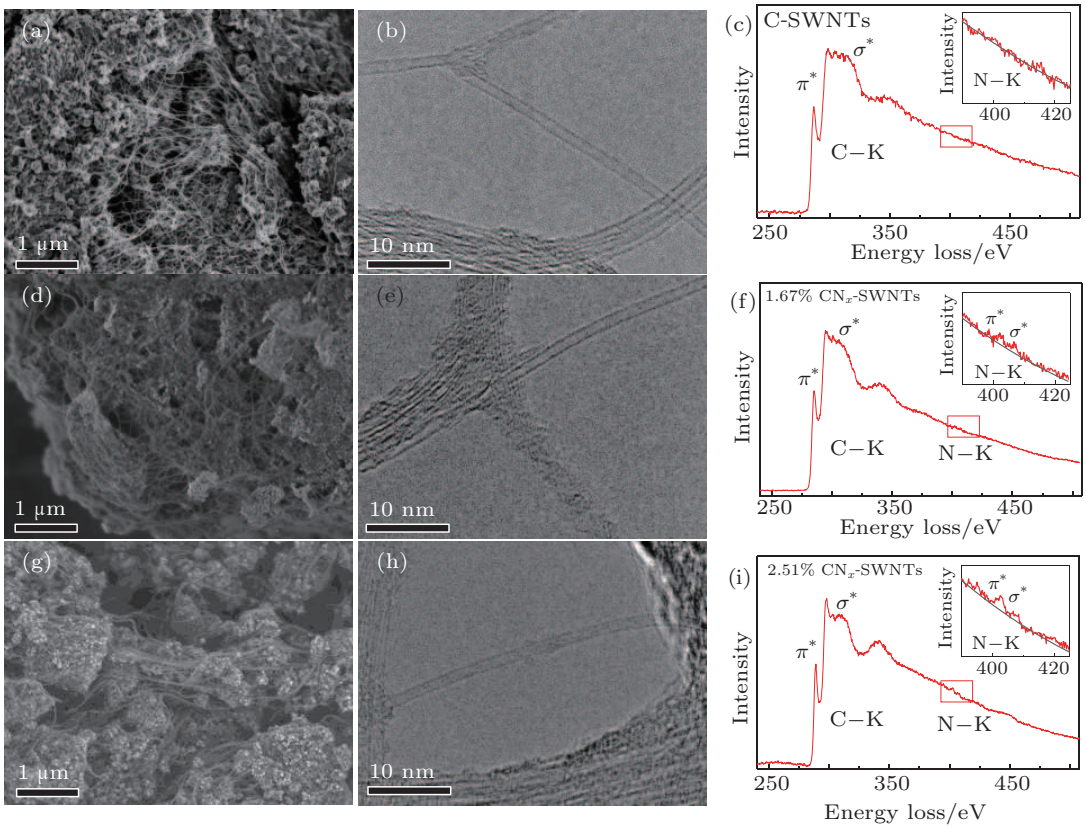


Fig. 1. (color online) Top panels show SEM (a), HR-TEM (b) images, and EELS spectrum (c) of the as-grown pure SWNTs. Middle panels show the SEM (d), HR-TEM (e) images, and EELS spectrum (f) of the as-grown N-doped SWNTs synthesized with CH_4:NH_3 of 9:1. Bottom panels show the SEM (g), HR-TEM (h) images, and EELS spectrum (i) of as-grown N-doped SWNTs synthesized with CH_4:NH_3 of 5:1.

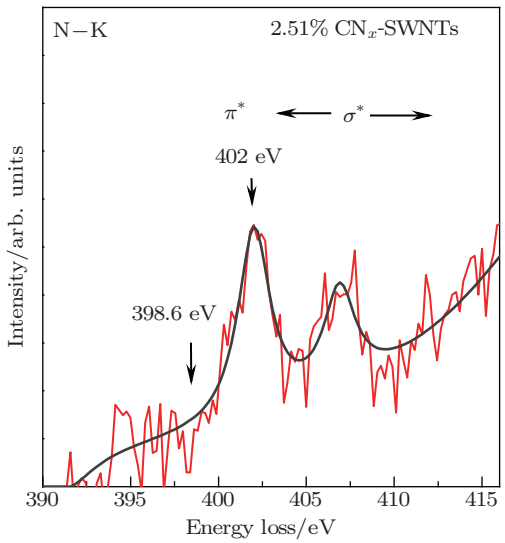


Fig. 2. (color online) Enlargement of the N–K edge after background subtraction of CN_x-SWNT with 2.51% nitrogen concentration. The π^* and σ^* fine structure features of the nitrogen K-edge can be clearly identified.

Raman spectroscopy is a key characterization method for carbon materials, especially carbon nanotubes and graphene.[14,19,28,29] They show common features in the range of 1000 cm^{-1}∼3000 cm^{-1}: the G band at around 1580 cm^{-1}, the D band at around 1350 cm^{-1}, and the overtone of D band (2D band) at around 2690 cm^{-1}. The G band corresponds to the E_{2g} phonon at the Brillouin-zone center (Γ point), and the D band is due to the breathing modes of sp^2 atoms and requires disorders (defects, doping, edges, etc.) for its activation. The 2D band, instead, which is symmetry-allowed, involves in-plane transversal optical (iTO) phonons near the Brillouin-zone boundary (K point), and is selected by the double-resonance process. Besides these Raman features, an additional radial breathing mode (RBM) located in the range of 100 cm^{-1}∼500 cm^{-1} can also be observed, for the case of SWNT systems. Figure 3(a) shows the Raman spectra of the as-grown C-SWNTs, and CN_x-SWNTs with nitrogen contents of 1.67 at% and 2.51 at%, respectively. The appearance of the RBM bands in all the three spectra is a fingerprint signal indicating the presence of SWNTs in these samples. While the C-SWNTs have an obscure disorder-induced D band, the CN_x-SWNTs have more prominent peaks of D band with increasing dopant concentrations, indicating that nitrogen doping breaks the spatial symmetry of the tube shell lattice.[14,29]

More importantly, apart from the symmetry-breaking effect, the doping induced charge defects can also renormalize the energies of the strongly coupled electrons and phonons near the doping sites. In CNT and graphene sys-

tems, electrons and phonons couple strongly and phonon softening via the Kohn anomaly can be observed at the K and Γ points.[16–19,30] As is well documented in theoretical and experimental studies of the electrostatic doping of CNTs and graphene by an external gate field, G band stiffening will always occur for both electron and hole doping due to the nonadiabatic removal of the Kohn anomaly from the Γ point, or the reduced electron screening of the C–C sp^2 bonds.[16–19] Note that the G band consists of higher (G^+) and lower (G^-) frequencies of both semiconducting and metallic nanotubes, which are respectively assigned to vibrations along the axial direction and the circumferential direction of a semiconducting nanotube, the opposite of the metallic case.[14] In this context, the sharp Lorentzian features of the peaks indicate the as-grown nanotubes probed by 2.33-eV laser excitation are mainly semiconducting, as shown in Fig. 3(b). The G^+ peak of semiconducting nanotubes, around 1590 cm^{-1}, is known to shift with electron or hole doping.[6,16,17] The discussion below for G band will focus only on the G^+ band of semiconducting nanotubes which is the main peak of the G band as can be seen from Fig. 3(b). Unlike the G band, the 2D band is much more strongly dependent on the particular electronic structure, and electron doping will cause a red-shift whereas the hole doping will cause a blue-shift.[15–19] Therefore, the 2D band can be used as a gauge for distinguishing the doping type. As can be seen from Fig. 3, the Raman spectra of CN_x-SWNTs clearly show blue-shift of the G band and red-shift of the 2D band, which demonstrates that the incorporation of nitrogen heteroatoms into the nanotube shell lattice introduces the n-type doping, as expected. Moreover, with a higher doping level, the Raman frequency shifts will increase accordingly. Figure 4 shows the measured shifts of Raman frequency as a function of dopant contents, and a nearly linear relationship can be deduced for both the blue-shifts of the G band frequency and the red-shifts of the 2D band frequency. As previously reported, an electron-injection density of about 5×10^6/cm corresponds to a G band blue shift of 5 cm^{-1}, and the shift is nearly linear with the electron-injection density at room temperature.[16] Thus the 3-cm^{-1} and 4.5-cm^{-1} Raman frequency shifts for G band of the CN_x-SWNT samples with 1.67 at% and 2.51 at% nitrogen contents correspond to an electron-injection density of $n \approx 3\times10^6$/cm and 4.5×10^6/cm, respectively.

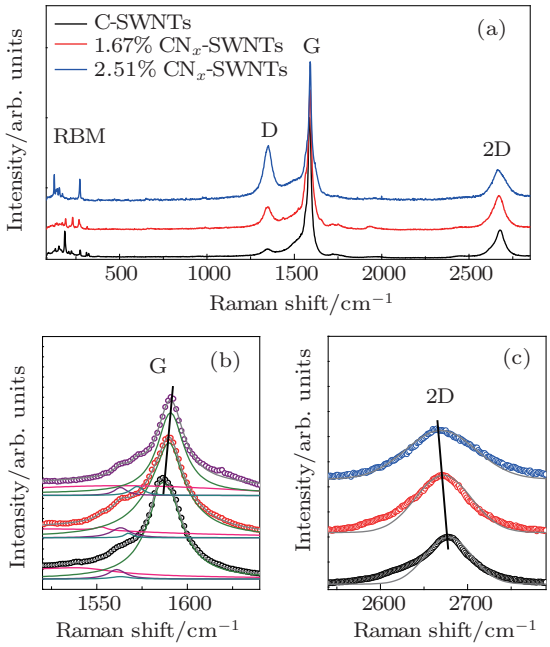


Fig. 3. (color online) (a) Raman scattering spectra recorded with a 2.33-eV laser excitation from the pristine and doped SWNTs. The panels (b) and (c) show the G and 2D regions of Raman responses.

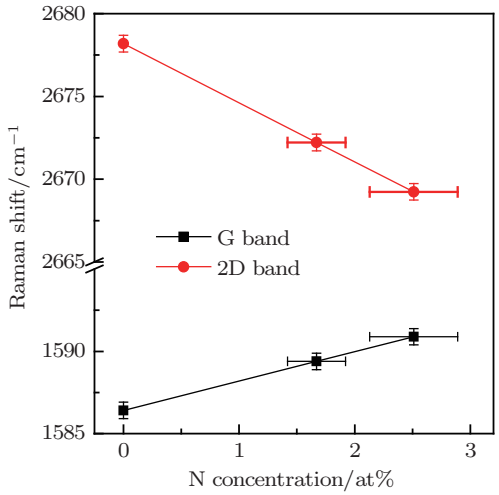


Fig. 4. (color online) Raman G and 2D peak positions of pristine and doped SWNTs as a function of nitrogen concentration.

In order to understand how the n-type doping occurs when the nitrogen heteroatoms are substitutionally incorporated into the honeycomb tube-shell carbon lattice, we performed density-functional theory (DFT) calculations on the distribution of the electron density. A semiconducting (10, 0) nanotube and a metallic (6, 6) nanotube were used here for modeling. We consider only the graphitic form of nitrogen dopants, since it was dominant in our as-grown CN_x-SWNTs samples (Fig. 2, as mentioned above). Before and after doping, the whole structures were fully optimized, including the positions of all the atoms and the sizes of the simulation cells. When one carbon atom was replaced by one nitrogen atom in the sp^2-hybridized super-cell, the structural change of the carbon network was negligible (the change of C–C bond length was smaller than 0.2% on average). For the (10, 0) C-SWNT, there are 40 carbon atoms in the supercell, and the substitution of one nitrogen atom for one carbon atom corresponds to a dopant concentration of 2.5 at%. The change of the electron density after doping is plotted in Fig. 5. The electron

density difference $\Delta\rho$ (unit: e/Å^3) is defined as $\Delta\rho = \rho$ (CN$_x$-SWNTs)$-\rho$ (C-SWNTs), where ρ (CN$_x$-SWNTs) is the electron density in the doped nanotubes and ρ (C-SWNTs) is the electron density in the pristine nanotubes. In order to show the $\Delta\rho$ clearly, we ignore the small structural change of the carbon network upon doping, which means the positions of carbon atoms in the C-SWNT are exactly the same as the carbon and nitrogen atoms in the CN$_x$-SWNTs. Four cross sections for the electron density perpendicular to the axis of the CNT are shown in Figs. 5(a), 5(b), 5(c), 5(d), and Figs. 5(e), 5(f), 5(g), and 5(h) display the top views of these cross sections, where the color green represents $\Delta\rho < 0$ (electron depletion) and the red represents $\Delta\rho > 0$ (electron gain). It can be clearly seen that the deep red circle in Fig. 5(e) corresponds to the nitrogen atom because it has one more electron than a carbon atom. One interesting finding here in all cross sections is that the carbon atoms are surrounded by both green and red electron clounds except the C–N bonded atoms, suggesting a charge polarization of carbon atoms due to nitrogen doping. As the position of carbon atom is moved farther from nitrogen dopant, the polarization becomes weaker. Nevertheless, the region of electron gain is always larger than that of electron depletion, which means there is a net electron transfer from the nitrogen dopant to the carbon network. The same conclusion can also be deduced from calculation results of the metallic (6, 6) SWNT (the calculated distribution of electron densities and difference electron densities of N-doped (6, 6) single-wall carbon nanotubes, see Fig. 6), where there are 24 carbon atoms in the supercell and one substitutional nitrogen atom which corresponds to a dopant concentration of 4.2 at%.

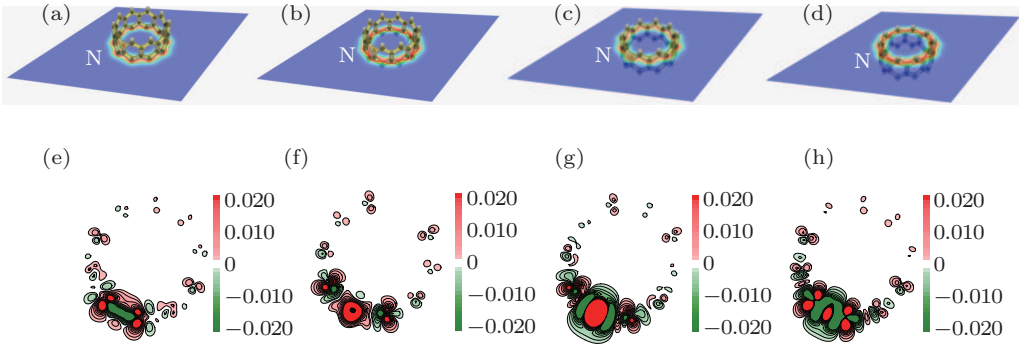


Fig. 5. (color online) Calculated distribution of the electron densities (ρ, in units of e/Å^3; the value of golden contour is 1.2 e/Å^3) of N-doped (10, 0) single-wall carbon nanotubes; here the indigotic planes characterize cross section perpendicular to tube central axis cross the first layer atoms (C1 cross section) (a), the second layer atoms (C2 cross section) (b), nitrogen atom (the third layer atoms, N cross section) (c), and the fourth layer atoms (C4 cross section) (d), respectively. Black atoms represent carbon and red atoms represent nitrogen. Colors show difference in electron densities ($\Delta\rho$, in units of e/Å^3, $\Delta\rho = \rho$ (CN$_x$-SWNT)–ρ (C-SWNTs)) of C1 cross section (e), C2 cross section (f), N cross section (g), and C4 cross section (h). Red represents the region of charge accumulation ($\Delta\rho > 0$) and green represents the region of charge depletion ($\Delta\rho < 0$).

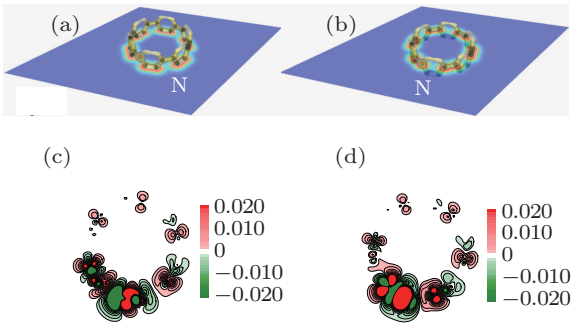


Fig. 6. (color online) Calculated distribution of the electron densities (ρ, in units of e/Å^3; the value of golden contour is 1.2 e/Å^3) of N-doped (6, 6) single-wall carbon nanotubes, here the indigotic planes characterize cross section perpendicular to tube central axis cross only carbon atoms (C cross section) (a) and nitrogen atoms (N cross section) (b), respectively. (color) Difference electron densities ($\Delta\rho$, in unit of e/Å^3, $\Delta\rho = \rho$ (CN$_x$-SWNTs)–ρ (C-SWNTs)) of C cross section (c) and N cross section (d). Red represents the region of charge accumulation ($\Delta\rho > 0$) and green represents the region of charge depletion ($\Delta\rho < 0$).

4. Conclusion

In summary, the bulk-quantity synthesis of CN$_x$-SWNTs with tunable dopant concentrations was achieved through a simple and conventional CVD growth procedure by employing CH_4 as the carbon source and NH_3 as the nitrogen source. The as-grown CN$_x$-SWNTs were characterized by SEM, TEM, EELS, and Raman spectroscopy. More importantly, the results of Raman scattering studies show that nitrogen doping leads to Raman G band phonon stiffening and 2D band phonon softening, which is a clear evidence of the n-type doping, indicating the doping-induced renormalization of the electron and phonon energies in the nanotubes. On the basis of first principles calculations of the distribution of delocalized carrier density in pristine and doped nanotubes, we show how the n-type doping occurs when nitrogen heteroatoms are substitutionally

incorporated into the honeycomb tube-shell carbon lattice.

References

[1] Arnold M S, Green A A, Hulvat J F, Stupp S I and Hersam M C 2006 *Nat. Nanotech.* **1** 60

[2] Liu C H, Liu Y Y, Zhang Y H, Wei R R and Zhang H L 2009 *Phys. Chem. Chem. Phys.* **11** 7257

[3] Bachilo S M, Balzano L, Herrera J E, Pompeo F, Resasco D E and Weisman R B 2003 *J. Am. Chem. Soc.* **125** 11186

[4] Li X L, Tu X M, Zaric S, Welsher K, Seo W S, Zhao W and Dai H J 2007 *J. Am. Chem. Soc.* **129** 15770

[5] Zheng L W, Hu L Q, Xiao X J, Yang F, Lin H and Guo T L 2011 *Chin. Phys. B* **20** 128502

[6] Maciel I O, Campos-Delgado J, Cruz-Silva E, Pimenta M A, Sumpter B G, Meunier V, López-Urías F, Muñoz-Sandoval E, Terrones H, Terrones M and Jorio A 2009 *Nano Lett.* **9** 2267

[7] Ayala P, Arenal R, Loiseau A, Rubio A and Pichler T 2010 *Rev. Mod. Phys.* **82** 1843

[8] Ayala P, Arenal R, Rümmeli M, Rubio A and Pichler T 2010 *Carbon* **48** 575

[9] Jin L, Fu H G, Xie Y and Yu H T 2012 *Chin. Phys. B* **21** 057901

[10] Susi T, Kaskela A, Zhu Z, Ayala P, Arenal R, Tian Y, Laiho P, Mali J, Nasibulin A G, Jiang H, Lanzani G, Stephan O, Laasonen K, Pichler T, Loiseau A and Kauppinen E I 2011 *Chem. Mater.* **23** 2201

[11] Liu Y, Jin Z, Wang J Y, Cui R L, Sun H, Peng F, Wei L, Wang Z X, Liang X L, Peng L M and Li Y 2011 *Adv. Funct. Mater.* **21** 986

[12] Monteiro F H, Larrude D G, Maia M, da Costa E H, Terrazos L A, Capaz R B and Freire F L Jr 2012 *J. Phys. Chem. C* **116** 3281

[13] Wang E G 2006 *J. Mater. Res.* **21** 2767

[14] Jorio A, Dresselhaus G and Dresselhaus M S 2008 *Carbon Nanotubes: Advanced Topics in Synthesis, Properties and Applications* (Berlin: Springer-Verlag)

[15] Maciel I O, Anderson N, Pimenta M A, Hartschuh A, Qian H H, Terrones M, Terrones H, Campos-Delgado J, Rao A M, Novotny L and Jorio A 2008 *Nat. Mater.* **7** 878

[16] Tsang J C, Freitag M, Perebeinos V, Liu J and Avouris Ph 2007 *Nat. Nanotech.* **2** 725

[17] Das A, Sood A K, Govindaraj A, Saitta A M, Lazzeri M, Mauri F and Rao C N R 2007 *Phys. Rev. Lett.* **99** 136803

[18] Pisana S, Lazzeri M, Casiraghi C, Novoselov K S, Geim A K, Ferrari A C and Mauri F 2007 *Nat. Mater.* **6** 198

[19] Das A, Pisana S, Chakraborty B, Piscanec S, Saha S K, Waghmare U V, Novoselov K S, Krishnamurthy H R, Geim A K, Ferrari A C and Sood A K 2008 *Nat. Nanotech.* **3** 210

[20] Wang W L, Bai X D, Xu Z, Liu S and Wang E G 2006 *Chem. Phys. Lett.* **419** 81

[21] Wang W L, Bai X D, Liu K H, Xu Z, Golberg D, Bando Y and Wang E G 2006 *J. Am. Chem. Soc.* **128** 6530

[22] Kresse G and Hafner J 1993 *Phys. Rev. B* **47** 558

[23] Kresse G and Furthmüller J 1996 *Phys. Rev. B* **54** 11169

[24] Perdew J P, Burke K and Ernzerhof M 1996 *Phys. Rev. Lett.* **77** 3865

[25] Kresse G and Joubert D 1999 *Phys. Rev. B* **59** 1758

[26] Monkhorst H J and Pack J D 1976 *Phys. Rev. B* **13** 5188

[27] Glerup M, Steinmetz J, Samaille D, Stéphan O, Enouz S, Loiseau A, Roth S and Bernier P 2004 *Chem. Phys. Lett.* **387** 193

[28] Rao A M, Eklund P C, Bandow S, Thess A and Smalley R E 1997 *Nature* **388** 257

[29] Dresselhaus M S, Dresselhaus G, Saito R and Jorio A 2005 *Phys. Rep.* **409** 47

[30] Piscanec S, Lazzeri M, Mauri F, Ferrari A C and Robertson J 2004 *Phys. Rev. Lett.* **93** 185503